Ultrafast carrier dynamics in Cu(In,Ga)Se$_2$ thin films probed by femtosecond pump-probe spectroscopy

Shih-Chen Chen,[1] Yu-Kuang Liao,[1,4] Hsueh-Ju Chen,[1] Chia-Hsiang Chen,[3] Chih-Huang Lai,[3] Yu-Lun Chueh,[3] Hao-Chung Kuo,[2] Kaung-Hsiung Wu,[1,*] Jenh-Yih Juang,[1] Shun-Jen Cheng,[1] Tung-Po Hsieh,[4] and Takayoshi Kobayashi[1]

[1]Department of Electro-Physics, National Chiao-Tung University, Hsinchu, Taiwan
[2]Department of Photonics and Institute of Electro-Optical Engineering, National Chiao-Tung University, Hsinchu, Taiwan
[3]Department of Materials Science and Engineering, National Tsing Hua University, Hsinchu, Taiwan
[4]Compound Semiconductor Solar Cell Department, Next Generation Solar Cell Division, Green Energy and Environment Research Laboratories, Industrial Technology Research Institute, Hsinchu, Taiwan
[*]khwu@cc.nctu.edu.tw

Abstract: Ultrafast carrier dynamics in Cu(In,Ga)Se$_2$ films are investigated using femtosecond pump-probe spectroscopy. Samples prepared by direct sputtering and co-evaporation processes, which exhibited remarkably different crystalline structures and free carrier densities, were found to result in substantially different carrier relaxation and recombination mechanisms. For the sputtered CIGS films, electron-electron scattering and Auger recombination was observed, whereas for the co-evaporated CIGS films, bandgap renormalization accompanied by band filling effect and hot phonon relaxation was observed. The lifetime of defect-related recombination in the co-evaporated CIGS films is much longer than that in the direct-sputtered CIGS films, reflecting a better quality with higher energy conversion efficiency of the former.

OCIS codes: (040.5350) Photovoltaic; (300.6530) Spectroscopy, ultrafast.

References and links

1. P. Jackson, D. Hariskos, E. Lotter, S. Paetel, R. Wuerz, R. Menner, W. Wischmann, and M. Powalla, "New world record efficiency for Cu(In,Ga)Se$_2$ thin-film solar cells beyond 20%," Prog. Photovolt. Res. Appl. **19**(7), 894–897 (2011).
2. M. Ganchev, J. Kois, M. Kaelin, S. Bereznev, E. Tzvetkova, O. Volobujeva, N. Stratieva, and A. Tiwari, "Preparation of Cu(In,Ga)Se$_2$ layers by selenization of electrodeposited Cu–In–Ga precursors," Thin Solid Films **511–512**, 325–327 (2006).
3. G. M. Hanket, W. N. Shafarman, B. E. McCandless, and R. W. Birkmire, "Incongruent reaction of Cu–(InGa) intermetallic precursors in H$_2$Se and H$_2$S," J. Appl. Phys. **102**(7), 074922 (2007).
4. V. Alberts, J. Titus, and R. W. Birkmire, "Material and device properties of single-phase Cu(In,Ga)(Se,S)$_2$ alloys prepared by selenizationy/sulfurization of metallic alloys," Thin Solid Films **451–452**, 207–211 (2004).
5. S. Chaisitsak, A. Yamada, and M. Konagai, "Preferred orientation control of Cu(In$_{1-x}$Ga$_x$)Se$_2$ (x ≈ 0.28) thin films and its influence on solar cell characteristics," Jpn. J. Appl. Phys. **41**(Part 1, No. 2A), 507–513 (2002).
6. C. H. Liu, C. H. Chen, S. Y. Chen, Y. T. Yen, W. C. Kuo, Y. K. Liao, J. Y. Juang, H. C. Kuo, C. H. Lai, L. J. Chen, and Y. L. Chueh, "Large scale single-crystal Cu(In,Ga)Se$_2$ nanotip arrays for high efficiency solar cell," Nano Lett. **11**(10), 4443–4448 (2011).
7. M. Nishitani, T. Negami, N. Kohara, and T. Wada, "Analysis of transient photocurrents in Cu(In,Ga)Se$_2$ thin film solar cells," J. Appl. Phys. **82**(7), 3572–3575 (1997).
8. B. Ohnesorge, R. Weigand, G. Bacher, A. Forchel, W. Riedl, and F. H. Karg, "Minority-carrier lifetime and efficiency of Cu(In,Ga)Se$_2$ solar cells," Appl. Phys. Lett. **73**(9), 1224–1226 (1998).
9. A. Othonos, "Probing ultrafast carrier and phonon dynamics in semiconductors," J. Appl. Phys. **83**(4), 1789–1830 (1998).
10. T. R. Tsai, C. F. Chang, and S. Gwo, "Ultrafast hot electron relaxation time anomaly in InN epitaxial films," Appl. Phys. Lett. **90**(25), 252111 (2007).

11. J. A. Kash, "Carrier-carrier scattering: An experimental comparison of bulk GaAs and GaAs/Al$_x$Ga$_{1-x}$As quantum wells," Phys. Rev. B Condens. Matter **48**(24), 18336–18339 (1993).
12. D. W. Snoke, "Density dependence of electron scattering at low density," Phys. Rev. B Condens. Matter **50**(16), 11583–11591 (1994).
13. A. Haug, "Carrier density dependence of Auger recombination," Solid-State Electron. **21**(11-12), 1281–1284 (1978).
14. T. Korn, A. Franke-Wiekhorst, S. Schnüll, and I. Wilke, "Characterization of nanometer As-clusters in low-temperature grown GaAs by transient reflectivity measurements," J. Appl. Phys. **91**(4), 2333–2336 (2002).
15. R. Ascázubi, I. Wilke, S. Cho, H. Lu, and W. J. Schaff, "Ultrafast recombination in Si-doped InN," Appl. Phys. Lett. **88**(11), 112111 (2006).

1. Introduction

Cu(In,Ga)Se$_2$ (CIGS) is commonly regarded as one of the most promising materials for low-cost and high efficiency solar cell [1]. Further improvement of the light-to-electricity efficiency of large-area thin films is undoubtedly an important step towards realizing the tremendous application potential of CIGS-based solar cells. Currently, CIGS films have been fabricated by non-vacuum processes (electrochemical deposition [2] and ink printing, both with post-selenization) and vacuum processes (co-evaporation, sputtering with/without post-selenization [3,4]). In order to boost the efficiency of CIGS thin films, the influences of deposition conditions practiced in various preparation processes on controlling the bandgap structure [3], defects, carrier concentration, film orientation [5], composition [5], and nanostructure [6] are under extensive investigations. Previous studies using transient photocurrent and time-resolved photoluminescence measurements have revealed that the efficiency of CIGS thin films is related to the lifetime of radiative recombination within the absorption layer [7,8], which can substantially affect the minority-carrier lifetime and hence the device performance. Therefore, it is essential to identify the defects related to the recombination traps and the mechanisms of the carrier relaxation processes in CIGS thin films. However, the above mentioned measurements only revealed the carrier lifetimes in the order of ns to μs [7,8], which are corresponding to the radiative recombination process, while the much faster carrier dynamics related to non-radiative recombination processes that limit the efficiency of the devices are rarely investigated and the associated lifetimes remain largely unknown.

Femtosecond pump-probe spectroscopy is a powerful tool for investigating the dynamics of nonequilibrium carriers in semiconductors. Ultrafast relaxation processes on the time scales of femtoseconds to picoseconds can be directly measured using this technique. In this letter, we report the study of ultrafast carrier relaxation dynamics in CIGS thin films by femtosecond optical pump-optical probe (OPOP) reflectivity measurements. The lifetimes for various relaxation and recombination processes were calculated by fitting the experimental curves. We found that the carrier relaxation and recombination mechanisms and their related lifetimes are significantly different in the samples prepared by various processes. These results provide important information for improving the efficiency of CIGS solar cells as well as in optimizing the film deposition conditions.

2. Experiments

The CIGS thin films investigated in this study were prepared by direct sputtering without post-selenization (sputtered CIGS) and conventional three-stage co-evaporation (co-evaporated CIGS) processes. A post-treatment utilizing KCN solution was performed to remove the Cu segregation and secondary phases in both samples.

For OPOP measurements, a commercial cavity-dumped Ti:sapphire laser system providing short pulses (~100 fs) with repetition rate of 5 MHz and wavelength of 800 nm (hν = 1.55 eV) was used. The power of the pump beam was varied from 10 to 60 mW and was focused at a diameter of about 35 μm. Thus, the corresponding pump fluence was ranging from 0.21 to 1.25 mJ/cm^2 while the probe fluence was fixed at 20 μJ/cm^2. The pump pulses were modulated at 2 KHz with chopper. A mechanical delay stage was used to vary the time delay

between the pump and probe pulses. The transient reflectivity change $\Delta R/R$ of the probe beam was measured as a function of the pump-probe delay time. The small reflected signals were detected and fed into a lock-in amplifier.

3. I-V characteristics and SEM images

Figures 1(a) and 1(b) show the typical I-V characteristics (IVCs) of the sputtered and co-evaporated CIGS samples, respectively. From the IVCs, the obtained V_{OC} (open-circuit voltage), J_{SC} (short-circuit current density), filling factor (FF), and solar efficiency (η) for the sputtered and co-evaporated CIGS samples are 0.50 V and 0.66 V, 24.58 mA/cm^2 and 25.81 mA/cm^2, 62% and 72%, and 7.61% and 12.35%, respectively. The results are summarized in Table 1. A lower V_{OC} for the sputtered CIGS is attributed to a smaller bandgap comparing to that of the co-evaporated CIGS, which has been confirmed by photoluminescence spectra (not shown here). Therefore, it was anticipated that the sputtered CIGS films should exhibit a higher J_{SC} than the co-evaporated CIGS films. Nevertheless, an opposite trend was observed. Namely, the J_{SC} of the sputtered CIGS is slightly lower than that of the co-evaporated CIGS. One of the possible reasons might be due to a higher defect concentration in the p-n junction of the sputtered CIGS that suppresses the J_{SC}. The insets show the corresponding SEM images of both CIGS absorption layers. It is evident that the two films display very different grain morphologies, with a columnar structure for the sputtered CIGS thin film while that for the co-evaporated CIGS films exhibits a coaxial grain structure. We suspect that columnar grain boundaries of the former may have played an important role in suppressing the J_{SC}. In addition, the lower FF exhibited in the sputtered CIGS comparing to that of the co-evaporated CIGS reflects a higher shunt leakage, which is also attributable to the columnar grain structure of the former. It appears that the columnar grain structure may have resulted in a higher concentration of recombination centers for the sputtered CIGS solar cells, which, in turn, yields a lower efficiency of 7.61% as compared to 12.35% obtained for the co-evaporated CIGS solar cells.
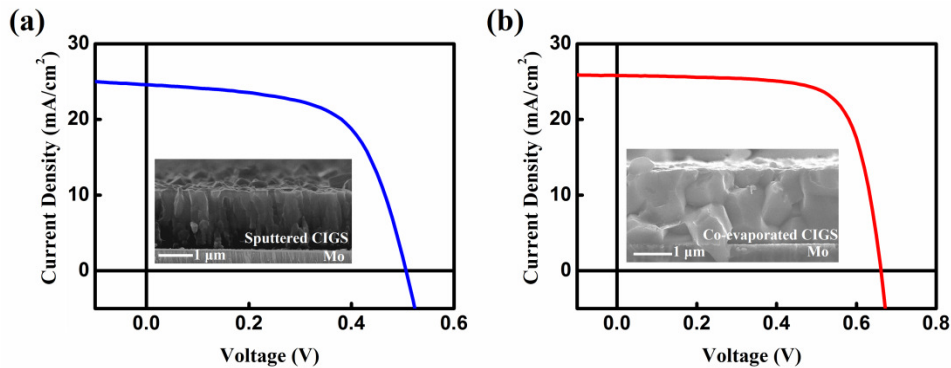

Fig. 1. I-V characteristics of CIGS solar cells prepared by (a) direct sputtering and (b) co-evaporation processes. Insets show the corresponding SEM images of the two samples.

Table 1. The photovoltaic parameters for direct sputtered and co-evaporated CIGS samples

	V_{oc} (V)	J_{sc} (mA/cm^2)	FF (%)	η (%)
Sputtered	0.50	24.58	62	7.61
Co-evaporated	0.66	25.81	72	12.35

4. Optical pump-optical probe measurements

In order to further elucidate the possible influences of the grain structure on the microscopic carrier dynamics in these CIGS films, we have carried out systematic OPOP investigations.

Figures 2(a) and 2(b) show the $\Delta R/R$ curves as a function of delay time measured at various pump fluences for sputtered and co-evaporated CIGS samples, respectively. Each $\Delta R/R$ curve displayed in Fig. 2(a) can be fitted by a bi-exponential decay while the $\Delta R/R$ curves displayed in Fig. 2(b) can be fitted by three exponential decays, including the quick rise of $\Delta R/R$ from negative to positive can be fitted by an exponential decay and the sequentially slow decay can be fitted by a bi-exponential decay. We will discuss the dominant relaxation and recombination processes for each sample from the distribution of $\Delta R/R$ curves and the fitting results of the carrier-density and pump-fluence dependences of magnitudes and relaxation time constants. As has been pointed out by A. Othonos [9], when the semiconductor is exposed to an ultrafast optical pulse with above band gap photon energy, many processes occur, including the generation of large nonequilibrium carrier densities, elevated carrier temperature, changes in the crystalline structure and band structure. This in turn will affect various macroscopic parameters such as the changes of dielectric constant, reflectivity, and transmission of the material. Moreover, the temporal and spatial evolutions of carrier relaxation and recombination processes are also very complicated. Therefore, the carrier-density, pump-fluence, probe-wavelength, and temperature dependences of the pump-probe results should be accurately analyzed to correctly delineate the mechanisms of ultrafast carrier dynamics prevailing in semiconductors.
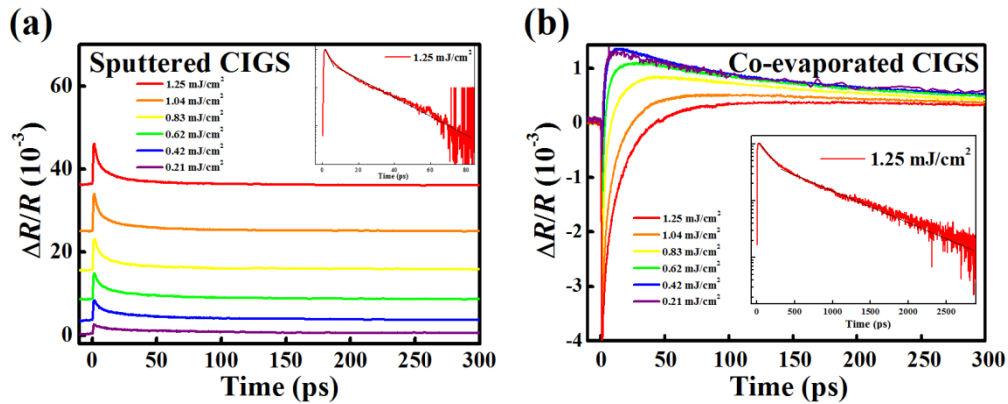

Fig. 2. (a) Reflectivity transient for the direct sputtered CIGS films. The inset shows the semi-log plot of the $\Delta R/R$ curve for a pump fluence of 1.25 mJ/cm^2. The curves were fitted with a biexponential decay function, $[A_1\exp(-t/\tau_{fast}) + A_2\exp(-t/\tau_{slow})]$. Where τ_{fast} is the characteristic cooling time of photoexcited hot carriers and τ_{slow} is related to carrier recombination. (b) The reflectivity transient for the co-evaporated CIGS films. The negative reflectivity in short delay time is due to the bandgap renormalization effect. The subsequent positive reflectivity transient decay fitted with a biexponential decay is originated from the fast process of the hot phonon relaxation, while the following slow process is due to the defect-related non-radiative recombination.

In order to discuss the mechanism of the fast relaxation process for the sputtered CIGS, the fast relaxation time (τ_{fast}) versus total carrier density was plotted and displayed in Fig. 3(a). Here we assume that the total carrier density is approximately equal to the photoexcited carrier density since the sputtered CIGS has a carrier density in the range of 10^{18} ~10^{19} cm^{-3} measured by Hall effect measurement, which is smaller than that of photoexcited carriers. For example, a total carrier density of 4.19×10^{19} cm^{-3} could be generated under a pump fluence of 0.21 mJ/cm^2. As shown in Fig. 3(a), τ_{fast} decreases from ~7.49 to ~3.76 ps as the total carrier density increases from ~4.19×10^{19} cm^{-3} to ~2.51×10^{20} cm^{-3} and reaches the plateau value of ~3.76 ps at the total carrier density larger than ~1.50×10^{20} cm^{-3}. One of the hot carrier relaxation channels at high electron concentration is that the hot electron energy loss through LO phonon emissions, which is called the hot phonon effect and the screening effect [9]. In this case, the electron relaxation time increases as the excitation density increases.

However, our measurement results obviously do not follow this expectation. This anomalous carrier density dependence is similar to those results reported by Tsai et al. [10], wherein the hot electron relaxation process in InN and GaAs has been attributed to electron-electron scattering [11,12]. Therefore, we may conclude that the dominant fast electron relaxation process in the sputtered CIGS films is the electron-electron scattering.

In order to interpret the slow relaxation process in the sputtered CIGS, the dependence of slow relaxation rate, $1/\tau_{slow}$, as a function of the total carrier density is shown in Fig. 3(b). A perfect linear fit (solid line) to the data can be obtained using an equation $1/\tau_{slow} = B_0 + B_2 n$ with $B_0 = 8.74 \times 10^9$ s^{-1} and $B_2 = 9.09 \times 10^{-11}$ cm^3 s^{-1}, respectively [10]. This result reveals that two recombination mechanisms are involved in the slow relaxation process. The linear carrier density dependence of the recombination rate for the later term $B_2 n$, is due to the Auger recombination process in degenerated carrier system and can be written as $1/\tau_{Aug}$ [13]. The B_2 suggests the Auger recombination lifetime, which is the order of picosecond magnitudes. It is much faster than the radiative recombination lifetime in the order of μs measured by time-resolved photoluminescence measurements. Another term B_0, which is independent of the total carrier density, is associated with the defect-related non-radiative recombination process. The defect-related non-radiative recombination lifetime, τ_n, is typically dominated by a so-called Shockley-Read-Hall mechanism at room temperature with $\tau_n = 1/(N_{def}\sigma_{def}v_{th})$. Where N_{def} is the density of defects, σ_{def} is their cross section, and v_{th} is the thermal velocity of the carriers [14]. The defect-related non-radiative recombination lifetime (τ_n) for this case is ~114 ps.
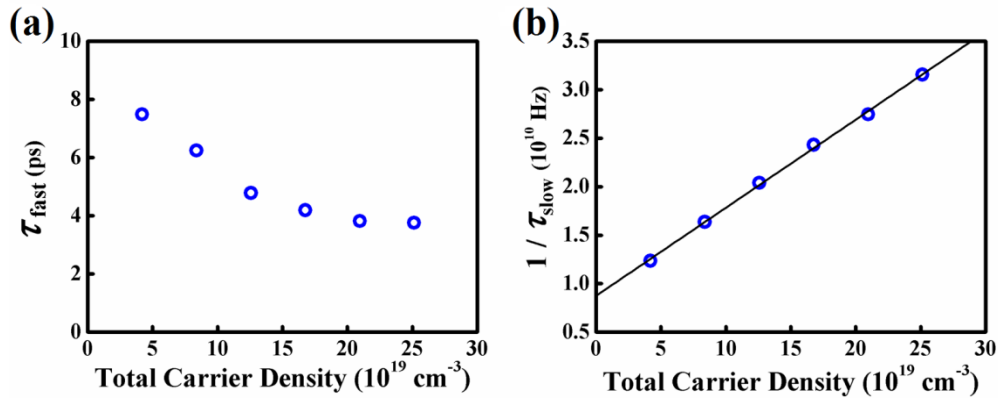

Fig. 3. (a) The extracted carrier cooling lifetime (τ_{fast}) in a short delay time under different carrier densities in the direct sputtered CIGS film. (b) The $1/\tau_{slow}$ extracted from the slower component in the biexponential decay function used to fit the reflectivity transient of the direct sputtered CIGS thin films.

In contrast, as shown in Fig. 2(b), the carrier relaxation behavior for the co-evaporated CIGS films, which with much lower free carrier density in the range of 10^{15} ~10^{16} cm^{-3}, is significantly different from those exhibited in sputtered CIGS films. Instead of displaying a steep increase upon pumping (Fig. 2(a)), each $\Delta R/R$ curve displayed in Fig. 2(b) exhibits a rapid drop in the initial stage, followed by a quick rise and then decays slowly with delay time. The temporal evolution of $\Delta R/R$ indicates that the carrier relaxation might have been dominated by effects of bandgap renormalization and band filling [15]. At a short delay time (within 1 ps), the band filling is still far from being saturated and the transient reflectance is dominated by the bandgap renormalization effect since the sample carrier density is much lower than that of photoexcited carriers, resulting in an abrupt decrease in $\Delta R/R$ signal. The fact that the amplitude of the negative $\Delta R/R$ signal increases with increasing pump fluence, suggesting a stronger bandgap renormalization effect resulted from a higher photoexcited carrier density at a higher pump fluence. As the carriers cool down and relax toward the band

edge, the change in absorption by band filling takes over the bandgap renormalization and leads to a sudden increase in reflectivity [15]. To further shed light on band filling effect, the τ_{fast} was extracted by fitting the $\Delta R/R$ signal to function $A_1\exp(-t/\tau_{\text{fast}})$ with a negative amplitude ($A_1 < 0$), as shown in Fig. 4(a). It is evident that, the extracted τ_{fast} from co-evaporated CIGS films is proportional to total carrier density, indicating that the dominant carrier relaxation in this case is due to the electron-phonon scattering during the band filling process [9]. Note that the carrier cooling mechanism in the co-evaporated CIGS films is different from that in the sputtered CIGS films. The cooling process in the co-evaporated CIGS film has eventually brought the amplitude of transient reflectivity back to positive, followed by a biexponational decay (see Fig. 2 inset), which can be attributed to a hot phonon relaxation and a defect-related non-radiative recombination. By carrying out the fitting analyses, it was observed that the hot phonon relaxation time was increased from 87 ps to 442 ps when the pump fluence was increased from 0.21 mJ/cm^2 to 1.25 mJ/cm^2. This can be understood as followings. Higher pump fluence is expected to result in a higher electron temperature, thereby transferring more energy to phonon. As a result, it would take longer time for the phonons to relax back to thermal equilibrium [9]. Another contribution to the biexponential decay is the defect-related non-radiative recombination characterized by a relaxation time constant, τ_{n}, which is largely independent of the total carrier density. Indeed, a constant value of ~750 ps for τ_{n} was obtained for the co-evaporated CIGS films at all carrier densities [15], as shown in Fig. 4(b). It is noted that this value is much longer than that obtained in sputtered CIGS films, which is 114 ps, indicating that the defect-related recombination rate in the co-evaporated CIGS films is significantly lower than that in sputtered CIGS films. Moreover, no Auger recombination was observed in the co-evaporated CIGS films, presumably due to a much lower carrier density in the co-evaporated CIGS film. Both are consistent with the notion that the columnar grain structure in the sputtered CIGS films is more defective and, hence, exhibits deteriorated conversion efficiency.
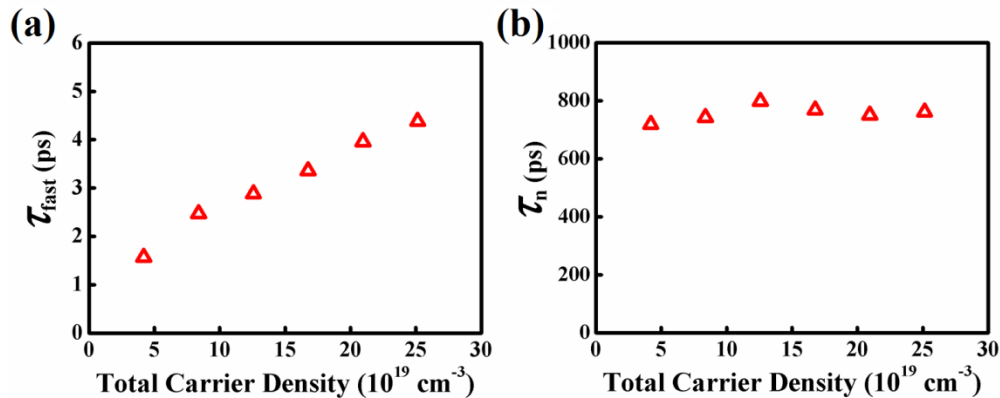

Fig. 4. (a) The extracted carrier cooling lifetime (τ_{fast}) in a short delay time under different carrier densities in the co-evaporated CIGS films. (b) The defect-related recombination lifetime (τ_{n}) as function of the total carrier density for the co-evaporated CIGS films.

5. Conclusion

In conclusion, the photovoltaic performance of Cu(In,Ga)Se$_2$ thin films prepared by direct sputtering and co-evaporation processes were compared, revealing the crucial role played by the resultant film microstructures. Systematic investigations of the ultrafast carrier dynamics in respective films were performed by femtosecond time-resolve pump-probe reflectivity measurements. The results demonstrate that the dominant carrier relaxation mechanism strongly depends on the carrier and defect densities in the samples while both can vary dramatically with different deposition processes. For the direct-sputtered CIGS films, the fast

relaxation time decreases with the increasing carrier density, which can be attributed to the electron-electron scattering dominated hot carrier relaxation. In contrast, for the co-evaporated CIGS films, the fast dynamics of carrier relaxation is dominated by electron-phonon scattering. On the other hand, the carrier density independent defect-related recombination rate in the co-evaporated CIGS film (τ_n ~750 ps) is much slower than that obtained from the sputtered CIGS film (τ_n ~114 ps) and no Auger recombination was observed in the former. These results indicate viable ways for further improving the photovoltaic efficiency of the CIGS-based solar cells as well as optimizing thin film deposition conditions.

Acknowledgments